

Low temperature pseudo-phase transition in an extended Hubbard diamond chain

Onofre Rojas and S. M. de Souza

Departamento de Física, Universidade Federal de Lavras, 37200-900, Lavras - MG, Brazil

Jordana Torrico,

*Departamento de Física, Universidade Federal de Minas Gerais,
C. P. 702, 30123-970, Belo Horizonte - MG, Brazil.*

L. M. Veríssimo, M. S. S. Pereira, and M. L. Lyra

Instituto de Física, Universidade Federal de Alagoas, 57072-970 Maceió - AL, Brazil

We consider the extended Hubbard diamond chain with an arbitrary number of particles driven by chemical potential. The interaction between dimer diamond chain and nodal couplings is considered in the atomic limit (no hopping), while the dimer interaction includes the hopping term. We demonstrate that this model exhibits a pseudo-transition effect in the low-temperature regime. Here, we explore the pseudo-transition rigorously by analyzing several physical quantities. The internal energy and entropy depict sudden, although continuous, jumps which closely resembles discontinuous or first-order phase transition. At the same time, the correlation length and specific heat exhibit astonishing strong sharp peaks, quite similar to a second-order phase transition. We associate the ascending and descending part of the peak with power-law "pseudo-critical" exponents. We determine the pseudo-critical exponents in the temperature range where these peaks are developed, namely $\nu = 1$ for the correlation length and $\alpha = 3$ for the specific heat. We also study the behavior of the electron density and isothermal compressibility around the pseudo-critical temperature.

I. INTRODUCTION

In recent investigations of several decorated one-dimensional models with short-range interactions, the first derivative of free energy, such as entropy, internal energy, and magnetization, shows a steep like function of temperature but still with continuous change which is quite similar to a first-order phase transition behavior. The second-order derivative of free energy, like the specific heat and magnetic susceptibility, resembles a typical second-order phase transition behavior at finite temperature. This peculiar behavior drew attention to a more careful study, as considered in reference [1]. In reference[2], an additional discussion of the above phenomenology focused in the behavior of correlation function for arbitrarily distant spins around the pseudo-transition. Similar pseudo-transitions were shown to take place in the Ising-Heisenberg diamond chain[3, 4] and even in the pure Ising diamond chain[5]. It also has been explored in the one-dimensional double-tetrahedral model, where the nodal sites are occupied by localized Ising spins and alternate with a pair of delocalized mobile electrons within a triangular plaquette[6]. Similarly, ladder model with alternating Ising-Heisenberg coupling[7], as well as the triangular tube model with Ising-Heisenberg coupling [8] depict pseudo-transition signatures. A universal character of pre-asymptotic pseudo-critical exponents has been demonstrated[9, 10]. These pseudo-transitions taking place at finite-temperatures in one-dimensional model systems with short-range interactions are of a distinct nature from the true phase-transition exhibited in the presence of long-range couplings for which the correlation length diverges, but e.g the specific heat can be without

divergence [11]. In all the above model systems presenting a pseudo-transition at finite temperature, one of the couplings was assumed to be Ising-like in order to allow for the exact calculation of the thermodynamic quantities. Examples of pseudo-transitions taking place in one-dimensional systems of interacting electrons without the assumption of an Ising-like nature of relevant couplings are still missing.

The Hubbard model is one of the simplest models that describe more accurately strongly interacting electron systems, which have attracted a great deal of interest over the past decades related to the possible emergence of geometrical frustration properties [12, 13]. Magnetic frustration in highly correlated electron models arises due to the geometric structure of the lattice, which induces system failures to satisfy simultaneously conflicting local requirements. The geometric frustration of Hubbard model has been extensively studied, particularly in the diamond chain structure, as considered by Derzhko et al.[14–16], where frustration for a particular class of lattice was discussed. Montenegro-Filho and Coutinho-Filho[17] also considered the doped AB_2 Hubbard chain, both in the weak coupling and the infinite- U limit (atomic limit) where quite interesting phases were identified as a function of hole doping away from the half-filled band, as well as 1/3-plateau magnetization, Kosterlitz-Thouless transition, and Luttinger liquid[18]. Further, Gulacsi et al.[19] also discussed the diamond Hubbard chain in a magnetic field and a wide range of properties such as flat-band ferromagnetism, correlation-induced metallic and half-metallic processes. The thermodynamics of the Hubbard model on a diamond chain in the atomic limit was discussed in reference [20]. Furthermore, frustrated quantum Heisenberg double-tetrahedral and octahedral chains

at high magnetic fields was discussed in[21]. Fermionic entanglement due to spin frustration was investigated in hybrid diamond chain with localized Ising spins and mobile electrons[22].

On the other hand, generally rigorous analysis of the Hubbard model is a challenging task. Only in a particular case it is possible to obtain exact results [23]. Earlier in the seventies, Beni and Pincus[24] focused in the one-dimensional Hubbard model. Later Mancini [25, 26] discussed several additional properties of extended one-dimensional Hubbard model in the atomic limit, obtaining the chemical potentials plateaus of the particle density, as a function of the on-site Coulomb potential at zero temperature. Earlier, the spinless versions of the Hubbard model on diamond chain also was investigated[27], as well as Lopes and Dias[28] performed a detailed investigation using the exact diagonalization approach. The Ising-Hubbard diamond chain has been investigated in reference [29]. In addition, experimental data regarding the 1/3 magnetization plateau in azurite[30, 31] were reproduced in several theoretical model systems such as the Ising-Heisenberg diamond chain[32–34]. The quantum block-block entanglement was investigated in the one-dimensional extended Hubbard model by exact diagonalization[35]. When the absolute value of the nearest-neighbor Coulomb interaction becomes small, the effects of the hopping term and the on-site interaction cannot be neglected. The experimental observation of the double peaks both in the magnetic susceptibility and specific heat [36–38] can be described accurately by the extended Hubbard diamond chain model without the hopping of electrons or holes between the nodal sites.

From an experimental point of view, the diamond chain structure is also motivating. Recently, the compound $\text{Cu}_3(\text{CH}_3\text{COO})_4(\text{OH})_5 \cdot 5\text{H}_2\text{O}$ has been synthesized [39], which exhibits a unique one-dimensional diamond chain structure. There are other compounds such as $\text{Cu}_3\text{Cl}_6(\text{H}_2\text{O})_2 \cdot 2\text{H}_8\text{C}_4\text{SO}_2$ trimer chain system[40], as well as the well known natural mineral azurite $\text{Cu}_3(\text{CO}_3)_2(\text{OH})_2$ [37] which are well represented by 1D diamond chains. These and similar compounds would be ideal physical systems on which pseudo-transitions at finite temperature could be searched.

Here, we advance in the study of pseudo-phase transitions in quasi one-dimensional systems by presenting a detailed exact study of the thermodynamic properties of the diamond chain Hubbard model in the atomic limit. The present article is organized as follow: In sec.2, we revisit the extended Hubbard model on diamond chain structure[20] with nodal sites considered in the atomic limit. In sec.3 we present our main findings where we focus in the existence of a pseudo-critical temperature by exploring the behavior of the correlation length. In sec.4 (sec.5) we analyze first (second) derivative physical quantities in the vicinity of the pseudo-transition. Finally, sec. 6 is devoted to our conclusions and perspectives.

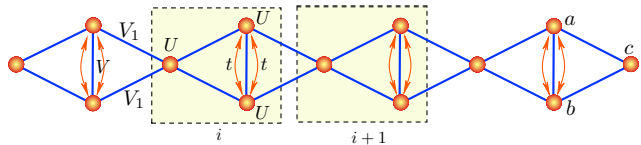


Figure 1: Schematic representation of the extended Hubbard model on the diamond chain. Onsite Coulomb repulsion interaction is denoted by U and nearest neighbor repulsion interaction is represented by V and V_1 , t stands for the electron hopping term.

II. THE EXTENDED HUBBARD MODEL

In this section, we revisit the model considered in reference [20]. Some results that will be used in the following section are updated and summarized. The model illustrated in fig.1, consider the hopping term t between sites a and b . Additionally, there is an onsite Coulomb repulsion interaction U and nearest neighbor repulsion interaction V between a and b , whereas V_1 corresponds the coupling between of nodal sites c with sites a and b (as labeled in the last block of fig.1). We also assume that this model has an arbitrary particle density. Thus, the system will be described by including a chemical potential denoted by μ . The Hamiltonian of the proposed model can be expressed by:

$$\mathbf{H} = \sum_{i=1}^N \mathbf{H}_{i,i+1}, \quad (1)$$

with N being the number of unit cells (sites a , b and c), and $\mathbf{H}_{i,i+1}$ is given by

$$\begin{aligned} \mathbf{H}_{i,i+1} = & -t \sum_{\sigma=\downarrow,\uparrow} \left(\mathbf{a}_{i,\sigma}^\dagger \mathbf{b}_{i,\sigma} + \mathbf{b}_{i,\sigma}^\dagger \mathbf{a}_{i,\sigma} \right) \\ & - \mu (\mathbf{n}_i^a + \mathbf{n}_i^b + \mathbf{n}_i^c) \\ & + U (\mathbf{n}_{i,\uparrow}^a \mathbf{n}_{i,\downarrow}^a + \mathbf{n}_{i,\uparrow}^b \mathbf{n}_{i,\downarrow}^b + \mathbf{n}_{i,\uparrow}^c \mathbf{n}_{i,\downarrow}^c) \\ & V \mathbf{n}_i^a \mathbf{n}_i^b + V_1 (\mathbf{n}_i^a + \mathbf{n}_i^b) (\mathbf{n}_i^c + \mathbf{n}_{i+1}^c), \end{aligned} \quad (2)$$

with $\mathbf{a}_{i,\sigma}$, and $\mathbf{b}_{i,\sigma}$ ($\mathbf{a}_{i,\sigma}^\dagger$ and $\mathbf{b}_{i,\sigma}^\dagger$) being the Fermi annihilation (creation) operators for electrons, while σ stands for the electron spin, and $\mathbf{n}_{i,\sigma}^\alpha$ stands for the number operator, with $\alpha = \{a, b, c\}$. Using this number operators, we also define conveniently the following operators $\mathbf{n}_i^\alpha = \mathbf{n}_{i,\uparrow}^\alpha + \mathbf{n}_{i,\downarrow}^\alpha$.

In order to contract and symmetrize the Hamiltonian (2), we can define properly the following operators

$$\begin{aligned} \mathbf{p}_{i,i+1} &= \frac{1}{2} (\mathbf{n}_i^c + \mathbf{n}_{i+1}^c), \\ \mathbf{q}_{i,i+1} &= \frac{1}{2} (\mathbf{n}_{i,\uparrow}^c \mathbf{n}_{i,\downarrow}^c + \mathbf{n}_{i+1,\uparrow}^c \mathbf{n}_{i+1,\downarrow}^c). \end{aligned} \quad (3)$$

Using these operators, we can rewrite the Hamiltonian (2), which becomes as follows:

$$\begin{aligned}
\mathbf{H}_{i,i+1} = & -t \sum_{\sigma=\downarrow,\uparrow} \left(\mathbf{a}_{i,\sigma}^\dagger \mathbf{b}_{i,\sigma} + \mathbf{b}_{i,\sigma}^\dagger \mathbf{a}_{i,\sigma} \right) - \mu \mathbf{p}_{i,i+1} \\
& - (\mu - 2V_1 \mathbf{p}_{i,i+1}) (\mathbf{n}_i^a + \mathbf{n}_i^b) + V \mathbf{n}_i^a \mathbf{n}_i^b \\
& + U (\mathbf{n}_{i,\uparrow}^a \mathbf{n}_{i,\downarrow}^a + \mathbf{n}_{i,\uparrow}^b \mathbf{n}_{i,\downarrow}^b) + U \mathbf{q}_{i,i+1}. \quad (4)
\end{aligned}$$

It is worth mentioning that this model already was investigated in reference [20], for arbitrary number of electrons. Here we consider in each site the following basis $\{0, \uparrow, \downarrow, \parallel\}$.

The eigenvalues and eigenvectors of the dimer plaquette are summarized in Table I, which are valid in general for arbitrary values of the Hamiltonian (1) parameters.

It is worth to mention that all analysis performed throughout this work will be done in the thermodynamic limit. Finite size effects can be evaluated in a similar way to that put forward in reference [41].

A. Phase Diagram

In order to analyze some relevant features, we will focus in the more interesting case when the particle-hole symmetry is satisfied which follows the restriction $V_1 = V/2$. Under this condition, for instance, we can analyze the half-filled band case, which occurs under the following restriction for the chemical potential $\mu = U/2 + 2V$.

It is worthy to mention that, the Hamiltonian (2), has 64 eigenvalues per diamond plaquette. The zero temperature phase diagram analysis was already discussed in reference [20]. Below we just give some ground-state energies relevant to the following analysis of the pseudo transition features.

Fig.2a illustrates the zero temperature phase diagram in the plane $t - \mu$, for fixed $U = 1$, $V = 0.1$ and $0 < \mu/U < 0.3$. There is a phase corresponding to a dimer antiferromagnetic (AFM_2) state,

$$|AFM_2\rangle = \prod_{i=1}^N |S_{\uparrow\downarrow}^{(-)}\rangle |0\rangle. \quad (5)$$

In this case, there are two electrons with opposite spins in the dimer sites, while nodal sites are empty. Thus, the electron density per unit cell is $\rho = 2/3$. The corresponding eigenvalue is given by

$$E_{AFM_2} = -2\mu + V - 2t \tan(\theta). \quad (6)$$

There is also a phase corresponding to a dimer and nodal frustrated state (FRU_2),

$$|FRU_2\rangle = \prod_{i=1}^N \frac{1}{\sqrt{2}} \left(\begin{vmatrix} 0 \\ \sigma_i \end{vmatrix} - \begin{vmatrix} \sigma_i \\ 0 \end{vmatrix} \right) |\tau_i\rangle. \quad (7)$$

This state also has two electrons: one electron is in a dimer site while the other occupies a nodal site, both

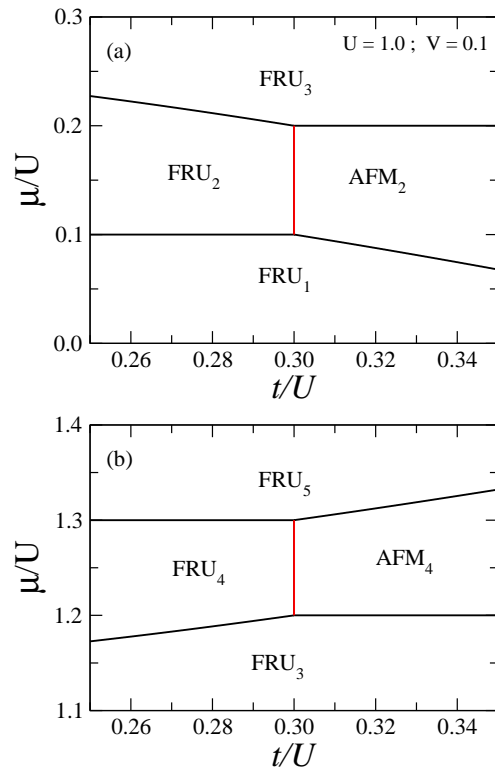


Figure 2: Zero temperature phase diagram in the plane $t - \mu$, assuming fixed $U = 1$, $V = 0.1$. (a) Shows the region of μ/U values where $\rho = 2/3$ phases appear; (b) The range of μ/U values where $\rho = 4/3$ phases appear.

with arbitrary spin orientation. The electron density $\rho = 2/3$. The corresponding residual entropy in units of k_B is $\mathcal{S} = \ln(4)$, whereas the ground-state energy becomes

$$E_{FRU_2} = -2\mu - t + V. \quad (8)$$

The vertical red line corresponds to $t_c = (U - V)/3 = 0.3$. We will focus in this phase boundary between $|AFM_2\rangle$ and $|FRU_2\rangle$. The corresponding interface residual entropy is $\mathcal{S} = \ln(4)$, as we will verify ahead.

Other surrounding states in the phase diagram are:

$$|FRU_1\rangle = \prod_{i=1}^N \frac{1}{\sqrt{2}} \left(\begin{vmatrix} \sigma \\ 0 \end{vmatrix} - \begin{vmatrix} 0 \\ \sigma \end{vmatrix} \right) |0\rangle \quad (9)$$

with $n = 1$ particle per unit cell and electron density $\rho = 1/3$.

$$|FRU_3\rangle = \prod_{i=1}^N \frac{1}{\sqrt{2}} \left(\begin{vmatrix} \parallel \\ 0 \end{vmatrix} - \begin{vmatrix} 0 \\ \parallel \end{vmatrix} \right) |\tau_i\rangle \quad (10)$$

with $n = 3$ electrons per unit cell or $\rho = 1$. The residual entropy in the frustrated phases (9) and (10) is given by $\mathcal{S} = \ln(2)$.

m	M_{ab}	Eigenvalues	g	Eigenvectors
0	0	$\lambda_{0,0} = \mathbf{D}_0$,	1	$ S_{00}\rangle = \begin{vmatrix} 0 \\ 0 \end{vmatrix}\rangle$
1	0.5	$\lambda_{0,\sigma}^{(\pm)} = \mathbf{D}_1 \pm t$	$\frac{2}{2}$	$ S_{0\sigma}^{(\pm)}\rangle = \frac{1}{\sqrt{2}} \left(\begin{vmatrix} 0 \\ \sigma \end{vmatrix} \mp \begin{vmatrix} \sigma \\ 0 \end{vmatrix} \right)$
2	1	$\lambda_{\sigma,\sigma} = \mathbf{D}_2 + V$	2	$ S_{\sigma\sigma}\rangle = \begin{vmatrix} \sigma \\ \sigma \end{vmatrix}\rangle$
	0	$\lambda_{0,\parallel}^{(1)} = \mathbf{D}_2 + U$	1	$ S_{0,\parallel}^{(1)}\rangle = \frac{1}{\sqrt{2}} \left(\begin{vmatrix} \parallel \\ 0 \end{vmatrix} - \begin{vmatrix} 0 \\ \parallel \end{vmatrix} \right)$
	0	$\lambda_{\uparrow\uparrow}^{(+)} = \mathbf{D}_2 + V + 2t \cot(\theta)$	1	$ S_{\uparrow\uparrow}^{(+)}\rangle = \frac{1}{\sqrt{2}} \left\{ \cos(\theta) \left(\begin{vmatrix} \parallel \\ 0 \end{vmatrix} + \begin{vmatrix} 0 \\ \parallel \end{vmatrix} \right) - \sin(\theta) \left(\begin{vmatrix} \uparrow \\ \downarrow \end{vmatrix} + \begin{vmatrix} \downarrow \\ \uparrow \end{vmatrix} \right) \right\}$
	0	$\lambda_{\uparrow\uparrow}^{(-)} = \mathbf{D}_2 + V - 2t \tan(\theta)$	1	$ S_{\uparrow\uparrow}^{(-)}\rangle = \frac{1}{\sqrt{2}} \left\{ \sin(\theta) \left(\begin{vmatrix} \parallel \\ 0 \end{vmatrix} + \begin{vmatrix} 0 \\ \parallel \end{vmatrix} \right) + \cos(\theta) \left(\begin{vmatrix} \uparrow \\ \downarrow \end{vmatrix} + \begin{vmatrix} \downarrow \\ \uparrow \end{vmatrix} \right) \right\}$
	0	$\lambda_{\downarrow,\uparrow}^{(2)} = \mathbf{D}_2 + V$	1	$ S_{\downarrow,\uparrow}^{(2)}\rangle = \frac{1}{\sqrt{2}} \left(\begin{vmatrix} \uparrow \\ \downarrow \end{vmatrix} - \begin{vmatrix} \downarrow \\ \uparrow \end{vmatrix} \right)$
3	0.5	$\lambda_{\parallel,\sigma}^{(\pm)} = \mathbf{D}_3 + U + 2V \pm t$	$\frac{2}{2}$	$ S_{\parallel,\sigma}^{(\pm)}\rangle = \frac{1}{\sqrt{2}} \left(\begin{vmatrix} \parallel \\ \sigma \end{vmatrix} \mp \begin{vmatrix} \sigma \\ \parallel \end{vmatrix} \right)$
4	0	$\lambda_{\parallel,\parallel} = \mathbf{D}_4 + 2U + 4V$	1	$ S_{\parallel,\parallel}\rangle = \begin{vmatrix} \parallel \\ \parallel \end{vmatrix}\rangle$

Table I: The first column means the number of particles in dimer plaquette, the second column describes the dimer plaquette magnetization, third column reports the eigenvalues, while fourth column corresponds to the eigenvalues degeneracy. The fifth column corresponds to the eigenvectors of dimer plaquette. Here $\mathbf{D}_m = -(\mu - 2V_1 \mathbf{p}_{i,i+1})m - \mu \mathbf{p}_{i,i+1} + U \mathbf{q}_{i,i+1}$ and $\cot(2\theta) = \frac{U-V}{4t}$.

Similarly, in fig.2b we show the phase diagram for the same set of fixed parameters but in the range $1.1 < \mu/U < 1.4$ where $\rho = 4/3$ phases appear.

In this region we observe also another dimer antiferromagnetic (AFM_4) state given by

$$|AFM_4\rangle = \prod_{i=1}^N |S_{\uparrow\uparrow}^{(-)}\rangle | \parallel \rangle, \quad (11)$$

where two electrons with opposite spins are located in the dimer sites, and the other pair of electrons is located in the nodal site. The respective ground-state energy becomes

$$E_{AFM_4} = -4\mu + 5V + U - 2t \tan(\theta). \quad (12)$$

There is also a dimer and nodal frustrated state (FRU_4),

$$|FRU_4\rangle = \prod_{i=1}^N \frac{1}{\sqrt{2}} \left(\begin{vmatrix} \parallel \\ \sigma_i \end{vmatrix} - \begin{vmatrix} \sigma_i \\ \parallel \end{vmatrix} \right) | \tau_i \rangle, \quad (13)$$

with corresponding ground-state energy

$$E_{FRU_4} = -4\mu - t + 5V + U, \quad (14)$$

and electron density $\rho = 4/3$.

The vertical red line corresponds to $t = (U - V)/3 = 0.3$. The phase boundary between $|AFM_2\rangle$ and $|FRU_2\rangle$

on which the residual entropy is $\mathcal{S} = \ln(4)$, as we will verify ahead.

The additional phase states illustrated in this diagram is composed by $n = 5$:

$$|FRU_5\rangle = \prod_{i=1}^N \frac{1}{\sqrt{2}} \left(\begin{vmatrix} \parallel \\ \sigma_i \end{vmatrix} - \begin{vmatrix} \sigma_i \\ \parallel \end{vmatrix} \right) | \parallel \rangle, \quad (15)$$

with $\rho = 5/3$. This frustrated phase has residual entropy $\mathcal{S} = \ln(2)$.

Further details of the ground state phase diagrams can be found in reference[20]. Pseudo-transitions are identified in the close vicinity of the $AFM_2 - FRU_2$ and $AFM_4 - FRU_4$ phase-boundaries.

B. Thermodynamics

In order to use the decoration transformation approach, we write the Boltzmann factors for the extended Hubbard model on diamond chain as follows:

$$\begin{aligned} w_{\mathbf{n}_i^c, \mathbf{n}_{i+1}^c} = & e^{-\beta \mathbf{D}_0} + 4 \left(e^{-\beta \mathbf{D}_1} + e^{-\beta(\mathbf{D}_3 + U + 2V)} \right) \cosh(\beta t) \\ & + e^{-\beta \mathbf{D}_2} \left(e^{-\beta U} + 3e^{-\beta V} \right) + e^{-\beta(\mathbf{D}_4 + 2U + 4V)} \\ & + e^{-\beta(\mathbf{D}_2 + V)} \left(e^{-\beta \vartheta + t/2} + e^{-\beta \vartheta - t/2} \right), \quad (16) \end{aligned}$$

with

$$\mathbf{D}_m = -(\mu - V\mathbf{p}_{i,i+1})m - \mu\mathbf{p}_{i,i+1} + U\mathbf{q}_{i,i+1}. \quad (17)$$

Here, ϑ_{\pm} is defined by

$$\vartheta_{\pm} = \frac{U - V \pm \sqrt{(U - V)^2 + 16t^2}}{t}. \quad (18)$$

To solve the effective Hubbard model with up to four-body coupling, we can use the transfer matrix method[42], similarly to that used in reference [24, 27]. Therefore the symmetric Hamiltonian by exchanging $i \rightarrow i + 1$ and $i + 1 \rightarrow i$, leads to a symmetric transfer matrix which can be expressed by:

$$\mathbf{W} = \begin{bmatrix} w_{0,0} & w_{0,1} & w_{0,1} & w_{0,2} \\ w_{0,1} & w_{1,1} & w_{1,1} & w_{1,2} \\ w_{0,1} & w_{1,1} & w_{1,1} & w_{1,2} \\ w_{0,2} & w_{1,2} & w_{1,2} & w_{2,2} \end{bmatrix}, \quad (19)$$

where the elements of \mathbf{W} is given by Eq. (16). Let us define a convenient notation,

$$w_{0,0}(x) = 1 + 2x \left(1 + \frac{x^2}{z^4 y^2} \right) \left(\frac{1}{\gamma^2} + \gamma^2 \right) + x^2 \left(\frac{3}{z^2} + \frac{1}{y^2} + \frac{1}{yz\zeta} + \frac{\zeta}{yz} \right) + \frac{x^4}{y^4 z^8}, \quad (20)$$

with $x = e^{\beta\mu}$, $y = e^{\frac{1}{2}\beta U}$, $z = e^{\frac{1}{2}\beta V}$, $\gamma = e^{\frac{1}{2}\beta t}$ and $\zeta = e^{\frac{1}{2}\beta\sqrt{(U-V)^2+16t^2}}$. All other Boltzmann factors could be expressed in terms of $w_{0,0}(x)$ defined by Eq. (20) as follows:

$$w_{n_1, n_2}(x) = \frac{x^{(n_1+n_2)/2}}{y^{\lfloor n_1/2 \rfloor} z^{\lfloor n_2/2 \rfloor}} w_{0,0} \left(\frac{x}{z^{n_1+n_2}} \right), \quad (21)$$

by $\lfloor \dots \rfloor$ we mean the floor function for any real number.

In order to carry out a reduced transfer matrix, we use the symmetry of the system. The proposed Hamiltonian is invariant with respect to electron spin orientation in nodal sites (site c). Therefore, the reduced transfer matrix becomes

$$\mathbf{V} = \begin{bmatrix} w_{0,0} & \sqrt{2}w_{0,1} & w_{0,2} \\ \sqrt{2}w_{0,1} & 2w_{1,1} & \sqrt{2}w_{1,2} \\ w_{0,2} & \sqrt{2}w_{1,2} & w_{2,2} \end{bmatrix}. \quad (22)$$

The determinant of the reduced transfer matrix becomes a cubic equation of the form

$$\det(\mathbf{V} - \Lambda) = (\Lambda^3 + a_3\Lambda^2 + a_2\Lambda + a_1) = 0, \quad (23)$$

where the coefficients become

$$\begin{aligned} a_1 &= 2w_{0,0}w_{1,2}^2 + 2w_{0,2}^2w_{1,1} + 2w_{0,1}^2w_{2,2} \\ &\quad - 2w_{0,0}w_{1,1}w_{2,2} - 4w_{0,2}w_{0,1}w_{1,2}, \\ a_2 &= 2w_{0,0}w_{1,1} + 2w_{1,1}w_{2,2} + w_{0,0}w_{2,2} \\ &\quad - 2w_{0,1}^2 - w_{0,2}^2 - 2w_{1,2}^2, \\ a_3 &= -w_{0,0} - 2w_{1,1} - w_{2,2}. \end{aligned} \quad (24)$$

Consequently, the roots of the algebraic cubic equation may be expressed as follow

$$\Lambda_j = 2\sqrt{Q} \cos\left(\frac{\phi - 2\pi j}{3}\right) - \frac{1}{3}a_3, \quad j = 0, 1, 2, \quad (25)$$

with

$$\phi = \arccos\left(\frac{R}{\sqrt{Q^3}}\right), \quad (26)$$

$$Q = \frac{a_3^2 - 3a_2}{9}, \quad (27)$$

$$R = \frac{9a_2a_3 - 27a_1 - 2a_3^3}{54}. \quad (28)$$

It is verified that $Q > 0$ in appendix A, which implies that all three roots must be different and real. We also analyze which eigenvalues must be the largest and the lowest one. So, it is enough to restrict $0 < \phi < \pi$ in the cubic solution without losing its general solution, as discussed in appendix A. Other intervals just exchange the cubic root solutions, as illustrated in table II. In the interval $0 < \phi < \pi$, the eigenvalues are ordered as $\Lambda_0 > \Lambda_1 > \Lambda_2$.

III. PSEUDO-CRITICAL TEMPERATURE

In this section we will analyze the anomalous thermodynamic property of the present extended diamond chain Hubbard model in the atomic limit[20]. In order to study the thermodynamic properties, we will use the exact free energy $f = -\frac{1}{\beta} \ln(\Lambda_0)$ as a starting point. Therefore, we will proceed our discussion of thermodynamic properties as a function of temperature and chemical potential. Particularly, we will analyze entropy, internal energy, correlation length, specific heat, electron density and isothermal compressibility. We aim to study physical quantities around the pseudo-critical temperature T_p . We stress that the present definition of "pseudo-critical" is different to that defined by Saito [43] to describe the critical-like behavior in approaching the spinodal point near the first order transition. Therefore, by using a perturbation approach, we can find the eigenvalues of transfer matrix (22), as discussed in Appendix B.

In general, pseudo-transitions can be manipulated and analyzed using perturbation techniques, as detailed in appendix B. For this purpose, we consider as unperturbed matrix \mathbf{V}_0 defined in appendix eq.(B1). The eigenvalues of the matrix B1, are given by (B2-B4), where we can observe the largest and second-largest eigenvalues are given by (B2) and (B3), respectively. However, in low temperature region we have the condition $w_{0,2} \ll \{w_{0,0}, w_{1,1}, w_{2,2}\}$. This is so because the leading term of $w_{0,2}$ comes from the lowest energy contribution of $w_{0,2}$ that includes only excited states, while the

leading term of $w_{0,0}$, $w_{1,1}$ and $w_{2,2}$ is given by the corresponding ground state energies of the system. Therefore, $w_{0,2}$ becomes exponentially small as compared to the other elements in the low-temperature regime. When (B2) and (B3) become eventually equal, we can get a pseudo-critical temperature from (B5), which reads

$$u_0^{(0)} = u_1^{(0)}. \quad (29)$$

Similar as discussed in [1], the relation (29) can induce us to believe that there is a true phase transition at finite temperature. However, the condition (29) does not mean that the transfer matrix eigenvalues satisfy $\Lambda_0 = \Lambda_1$: the condition (29) is satisfied only when the matrix (B8) is ignored and for $w_{0,2} = 0$. Therefore, the first order perturbative corrections (see eqs.(B9) and (B11)) are $u_0^{(1)} > 0$ and $u_1^{(1)} < 0$, which implies that the approximate solution given in (B12) must satisfy $\Lambda_0 > \Lambda_1$.

Returning to the relation (29), we get the following equation

$$w_{0,0} = 2w_{1,1} \quad \text{for } w_{0,0} > w_{2,2}, \quad (30)$$

and this one corresponds to the vicinity of the boundary line between AFM_2 and FRU_2 . The pseudo-critical temperature T_p is illustrated in fig.3a where we plot $T_p \times 10^{-3}$ (red line) as a function of chemical potential μ , for fixed parameters $t = 0.303$, $U = 1$ and $V = 0.1$. In fig.3b we report T_p for other values of t .

Similarly, the relation (29) leads to the following equation

$$w_{2,2} = 2w_{1,1}, \quad \text{for } w_{0,0} < w_{2,2}, \quad (31)$$

which holds in the close vicinity of the $FRU_4 - AFM_4$ boundary-line.

In fig.3a, we illustrate the pseudo-critical temperature $T_p \times 10^{-3}$ as a function of chemical potential μ . The continuous line corresponds to the pseudo-transition that occurs at low chemical potentials for which there are nearly 2 electrons per unit cell (near the boundary between AFM_2 and FRU_2 phases). The dashed line accounts for the second pseudo-transition appearing at larger chemical potential for which there are 4 electrons per unit cell in the ground-state (near the boundary between AFM_4 and FRU_4 phases). In this latter case, the chemical potential was conveniently shifted to $\mu - V - U = \mu - 1.1$ (top scale) to allow representing both pseudo-transitions in the same frame.

In panel (b) the pseudo-critical temperatures $T_p \times 10^{-2}$ as a function of t , for $\mu = 0.18$ (red line) and $\mu = 1.28$ (blue line) are illustrated. The pseudo-critical temperature vanishes linearly $T_p \propto (t - t_c)$ as one approaches the boundary-line $t_c = (U - V)/3$ from above, i.e., within one of the AFM ground-states.

A. Correlation length

Since the eigenvalues are non-degenerate, the correlation length ξ can be obtained by using the largest Λ_0

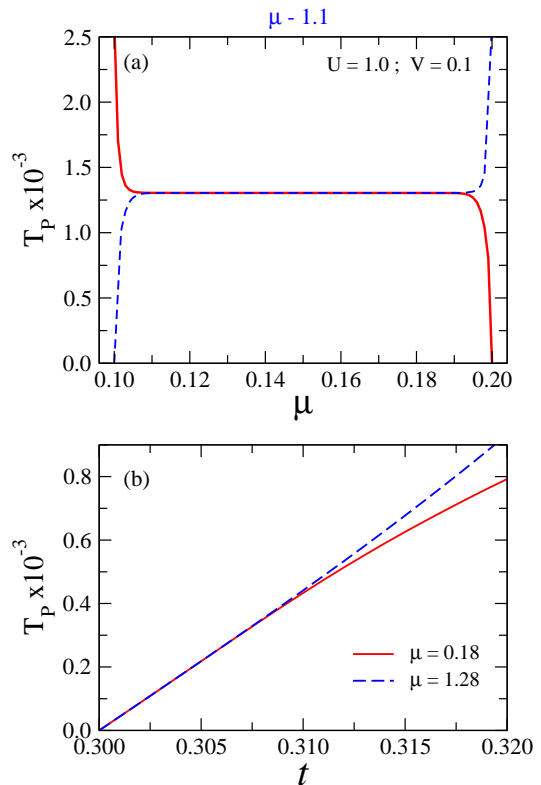


Figure 3: (a) Pseudo-critical temperature $T_p \times 10^{-3}$ for fixed parameters $t = 0.303$, $U = 1$ and $V = 0.1$ near AFM_2 and FRU_2 phases boundary (solid line) and near the AFM_4 and FRU_4 phases boundary (dashed line). In the latter the chemical potential was shifted to $\mu - 1.1$ (top scale). (b) Pseudo-critical temperature $T_p \times 10^{-2}$ as a function of t for $\mu = 0.18$ (solid line) and $\mu = 1.28$ (dashed line).

and second largest Λ_1 eigenvalues given from (25). It is simply written as

$$\xi = \left[\ln \left(\frac{\Lambda_0}{\Lambda_1} \right) \right]^{-1}. \quad (32)$$

In fig. 4 we illustrate the correlation length as a function of temperature. Panel (a) reports data for several values of t and assuming fixed $\mu = 0.18$, $U = 1$ and $V = 0.1$. Here we observe how the peak becomes more pronounced when $t \rightarrow t_c = (U - V)/3 = 0.3$ (approaching the $FRU_2 - AFM_2$ ground-state phase-boundary). For larger t the height of the peak becomes lower and broader. For $t = 0.303$ we already observe a strong peak around T_p , which was computed with high precision to be $T_p = 1.3046184136496 \times 10^{-3}$. Similarly, panel (b) reports for the same parameters set used in (a) but for $\mu = 1.28$ (in the vicinity of the $FRU_4 - AFM_4$ phase-boundary).

There are two situations where pseudo-transition occurs. The first one satisfy the condition $w_{0,0} \sim 2w_{1,1}$ but in the perturbation regime for which $8w_{0,1}^2 \ll (w_{0,0} - 2w_{1,1})^2$. Under this condition, we have the following re-

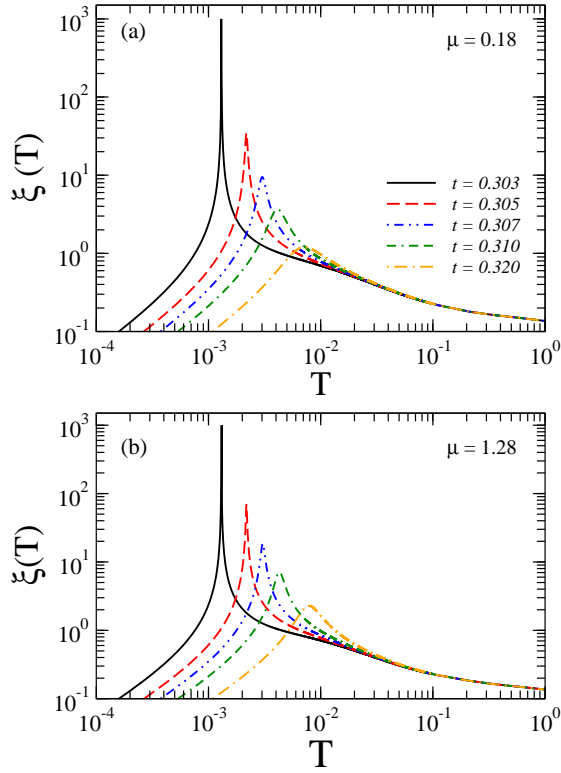


Figure 4: Correlation length as a function of temperature in logarithmic scale for fixed $U = 1$ and $V = 0.1$. (a) For several values of t , and fixed $\mu = 0.18$ (in the vicinity of the $FRU_2 - AFM_2$ phase-boundary). (b) For several values of t , and fixed $\mu = 1.28$ (in the vicinity of the $FRU_4 - AFM_4$ phase-boundary).

sult,

$$\frac{\Lambda_0}{\Lambda_1} \rightarrow \begin{cases} \frac{w_{0,0}}{2w_{1,1}}, & w_{0,0} > 2w_{1,1} \\ \frac{2w_{1,1}}{w_{0,0}}, & w_{0,0} < 2w_{1,1} \end{cases}. \quad (33)$$

Consequently, in the regime where the perturbation approach stands, the correlation length in the close vicinity of the pseudo-critical temperature can be expressed by

$$\xi_0(\tau) = c_{0,\xi} |\tau|^{-1} + \mathcal{O}(\tau^0). \quad (34)$$

Here $\tau = (T - T_p)/T_p$ and the coefficient is given by

$$c_{0,\xi} = \frac{\tilde{w}_{0,0}}{T_p \tilde{v}_0}, \quad (35)$$

with $\tilde{w}_{0,0}$ is $w_{0,0}$ evaluated at $T = T_p$, and

$$\tilde{v}_0 = \left| \frac{\partial (w_{0,0} - 2w_{1,1})}{\partial T} \right|_{T_p}. \quad (36)$$

Similarly, the second pseudo-transition occurs when $w_{2,2} \sim 2w_{1,1}$ but in the perturbation regime $8w_{1,2}^2 \ll$

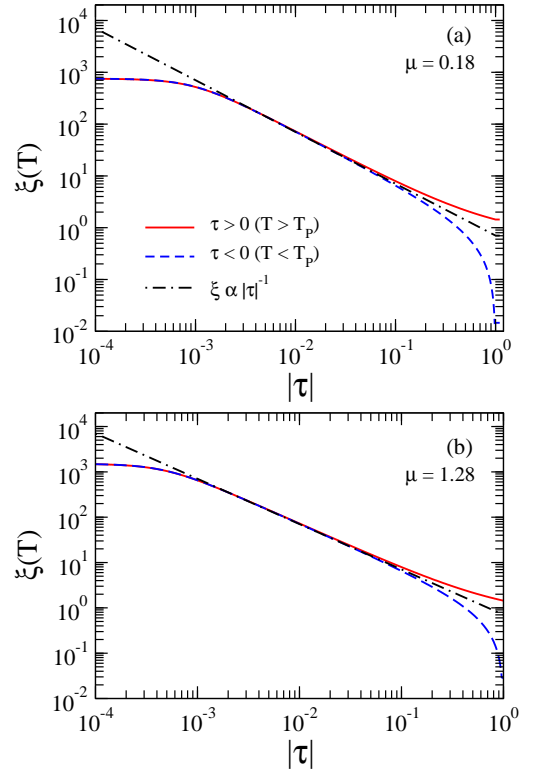


Figure 5: Correlation length as a function of τ , for fixed parameters $U = 1$, $V = 0.1$, $t = 0.303$. Red line corresponds for $\tau > 0$ ($T > T_p$) and dashed blue line denotes $\tau < 0$ ($T < T_p$), while straight dash-dotted line reports $\xi \propto |\tau|^{-1}$. (a) For $\mu = 0.18$. (b) For $\mu = 1.28$.

$(w_{2,2} - 2w_{1,1})^2$, that provides us

$$\frac{\Lambda_0}{\Lambda_1} \rightarrow \begin{cases} \frac{w_{2,2}}{2w_{1,1}}, & w_{2,2} > 2w_{1,1} \\ \frac{2w_{1,1}}{w_{2,2}}, & w_{2,2} < 2w_{1,1} \end{cases}. \quad (37)$$

Analogously, the correlation length close to the pseudo-transition, can be expressed around T_p , resulting in

$$\xi_2(\tau) = c_{2,\xi} |\tau|^{-1} + \mathcal{O}(\tau^0), \quad (38)$$

where the coefficient is given by

$$c_{2,\xi} = \frac{\tilde{w}_{2,2}}{T_p \tilde{v}_2}. \quad (39)$$

with $\tilde{w}_{2,2}$ evaluated at $T = T_p$, and

$$\tilde{v}_2 = \left| \frac{\partial (w_{2,2} - 2w_{1,1})}{\partial T} \right|_{T_p}. \quad (40)$$

These pre-asymptotic power-laws fail for very small τ , because the perturbation conditions can not be satisfied at T_p . Therefore, the correlation length actually depicts a pronounced peak and not a true divergence.

In fig.5a the correlation length is depicted as a function of τ in logarithmic scale, assuming fixed parameters $U = 1$, $V = 0.1$, $t = 0.303$ and $\mu = 0.18$. The solid curve represents $\tau > 0$ ($T > T_p$) while the dashed curve denotes $\tau < 0$ ($T < T_p$). The straight dash-dotted line reports the asymptotic limit $\xi \propto |\tau|^{-1}$, where we observe clearly the critical exponent $\nu = 1$ in the pseudo-critical regime. Notice that when T is very close to T_p the power law critical exponent fails, evidencing the ultimate non-singular behavior of the thermodynamic quantities. A similar plot is depicted in fig. 5b, assuming the same set of parameters but for chemical potential $\mu = 1.28$. Here again we observe manifestly the critical exponents $\nu = 1$. Note that the power-law behavior holds for nearly two decades.

In order to have a clear picture of the range of temperatures around T_p on which the pseudo-critical regime holds, we can estimate crossover boundaries between the non-singular and power-law regimes, as well as between the power-law regimes and the low and high temperature ones. The non-singular regime in the close vicinity of T_p emerges as the perturbation analysis fails. In the vicinity of the $FRU_2 - AFM_2$ ground-state transition, crossover lines can be built using $8w_{0,1}^2 = (w_{0,0} - 2w_{1,1})^2$, which separates the perturbative from the non-perturbative regimes. A similar crossover line can be written in the vicinity of the $FRU_4 - AFM_4$ ground-state transition [$8w_{1,2}^2 = (w_{2,2} - 2w_{1,1})^2$]. The power-law regime holds while the correlation length remains much larger the lattice spacing. We will consider that crossover lines from the power-law to the low and high-temperature regimes satisfies $\xi = 10$. Eqs. (32) and (33) can be used to draw the respective crossover lines.

In fig.6 we show the above crossover lines as a function the hopping parameter t in the close vicinity's of the $FRU_2 - AFM_2$ and $FRU_4 - AFM_4$ boundary lines for an illustrative set of the other Hamiltonian parameters. Firstly notice that the width of the non-singular regime decreases quite fast as one approaches $t_c = (U - V)/3$. While the pseudo-transition temperature T_p decreases linearly, the non-singular temperature range decays much faster as $e^{-a/(t-t_c)}$, with a being a constant at t_c . The non-singular regime widens as we further depart from t_c . On the other hand, the crossover lines to the high and low-temperature regimes are weakly dependent on t . Therefore, in the close vicinity of t_c , the power-law regime extends over a temperature range of the order of a few percents of T_p . The crossover lines delimiting the non-singular and the high and low temperature regimes eventually meet. After this point, no pre-asymptotic power-law regime can be identified.

IV. FIRST-ORDER LIKE PSEUDO-TRANSITION

It is interesting to analyze some physical quantities, which are obtained as a first derivative of the free energy

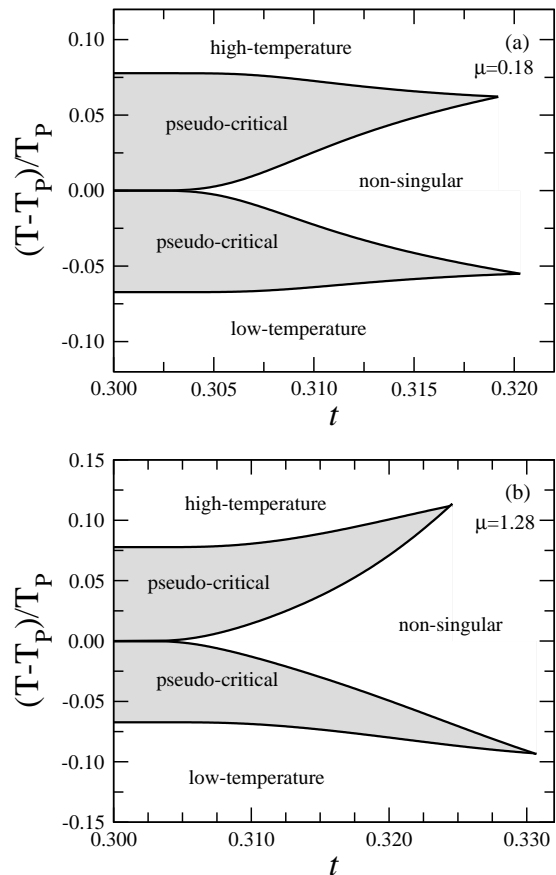


Figure 6: Distinct temperature regimes as a function of the hopping parameter t in the close vicinity of the $FRU_2 - AFM_2$ (a) and $FRU_4 - AFM_4$ (b) ground-state transitions. Here we used $U = 1$, $V = 0.3$, (a) $\mu = 0.18$ and (b) $\mu = 1.28$. The non-singular regime becomes exponentially narrow as $t \rightarrow t_c = (U - V)/3 = 0.3$. The power-law regime holds for $\tau = (T - T_p)/T_p$ of the order of a few percents in the close vicinity of t_c . It dies away far from t_c when the perturbation and large correlation length conditions become incompatible.

and exhibit an almost step-like behavior.

A. Entropy

In fig.7a we illustrate the density plot of entropy ($S = -\frac{\partial f}{\partial T}$) in the plane $t - \mu$, for fixed parameters $V = 0.1$, $U = 1$ and $T = 0.005$, for $\mu = [0, 0.3]$. This plot is depicted in the same scale of the phase diagram illustrated in fig.2a. We definitely observe a pseudo-transition in the boundary of quasi-antiferromagnetic $qAFM_2$ and quasi-frustrated $qFRU_2$ phases characterized by a sharp boundary, while electron density remains constant $\rho = 2/3$. The regions are mostly governed by the zero temperature phases but, due to thermal fluctuations, the zero temperature phases become "quasi" long-ranged because of the lack of actual spontaneous long-range order at any finite temperature. A similar

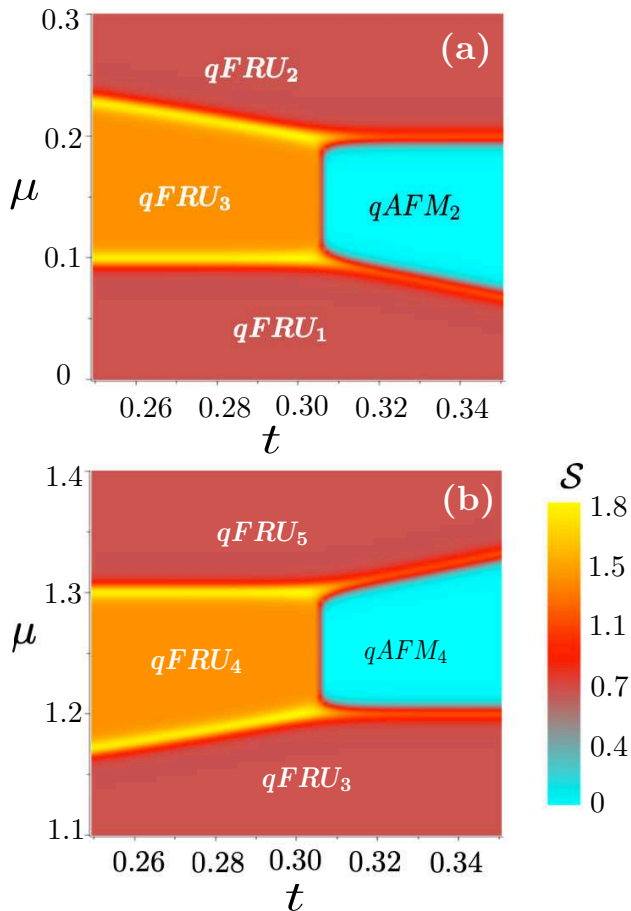


Figure 7: Density plot of entropy in the plane $t - \mu$, assuming fixed $V = 0.1$, $U = 1$ and $T = 0.005$. (a) For $\mu = [0, 0.3]$. (b) For $\mu = [1.1, 1.4]$.

density plot is illustrated in fig.7b, assuming the same parameters but in the interval of $\mu = [1.1, 1.4]$. We can observe a steep entropy change in the boundary between the $qAFM_4$ and $qFRU_4$ phases where the electron density $\rho = 4/3$ per cell remains unaltered.

In fig.8a we report the magnitude of entropy as a function of temperature in semi-logarithmic scale, assuming fixed parameters $t = 0.303$, $\mu = 0.18$, $U = 0.1$. Clearly one can observe a nearly step behavior at $T_p = 1.3 \times 10^{-3}$. For temperatures below T_p the entropy is almost null, which corresponds to the quasi-antiferromagnetic phase ($qAFM_2$). On the other hand, the entropy has a plateau region ($qFRU_2$) with $\mathcal{S}_0 = \ln(4)$ for $T > T_p$. As the temperature is further increased, the entropy behaves like in standard models. Therefore we observe a strong continuous change of entropy around the pseudo-transition, which typically resembles a discontinuous (first-order) phase transition. However, we stress that it remains analytical at T_p .

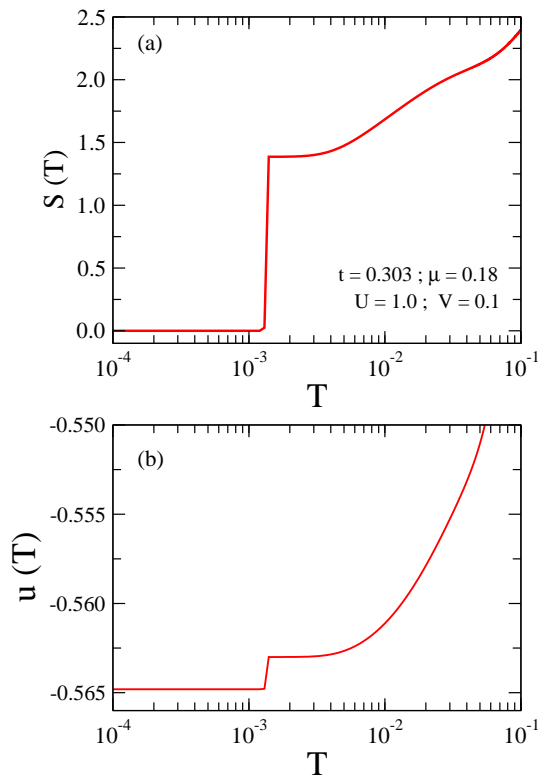


Figure 8: (a) Entropy as a function of temperature in semi-logarithmic scale, for fixed $t = 0.303$, $\mu = 0.18$, $U = 1$ and $V = 0.1$. (b) Internal energy as a function of temperature in semi-logarithmic scale, for fixed $t = 0.303$, $\mu = 0.12$, $U = 1$ and $V = 0.1$.

B. Internal energy

Other quantity we discuss here is the internal energy $u(T) = T\mathcal{S} + f$, which can also be obtained after a first-derivative of the free-energy.

In fig.8b, the internal energy as a function of temperature in semi-logarithmic scale is depicted, for fixed $t = 0.303$, $\mu = 0.18$, $U = 1$ and $V = 0.1$. Internal energy is continuous as a function of temperature, although it also shows a steep variation around the pseudo-critical temperature T_p . For temperatures below T_p , the internal energy leads to $u = -0.5648$, which corresponds to the AFM_2 ground state energy E_{AFM_2} . For $T > T_p$, the internal energy is mostly dominated by the FRU_2 ground-state energy $E_{FRU_2} = -0.563$.

C. The electron density

Another important quantity we explore is the thermal average electron density $\rho = -\left(\frac{\partial f}{\partial \mu}\right)$ per unit cell.

In fig.9 the electron density as function of temperature is reported in semi-logarithmic scale, for fixed $t = 0.303$, $U = 1$, $V = 0.1$ and $\mu = 0.12$. At low temperatures,

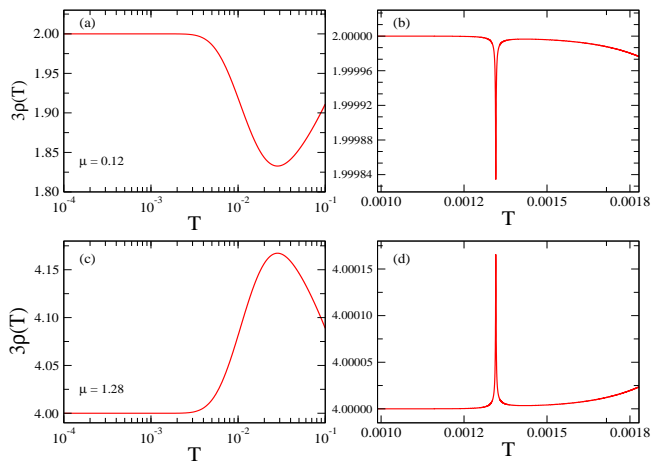


Figure 9: Electron density as a function of temperature in semi-logarithmic scale, for fixed $t = 0.303$, $U = 1$ and $V = 0.1$. (a) For $\mu = 0.12$. (b) Zooming panel (a) around T_p . (c) For $\mu = 1.28$. (d) Zooming panel (c) around T_p .

the electron density remains almost constant $\rho = 2/3$, up to roughly around $T \sim 0.01$, and then the electron density decreases to $3\rho \approx 1.80$, for higher temperature the electron density increases with temperature (for further details see reference [20]). Therefore apparently no pseudo-critical behavior at T_p is evidenced in ρ . In fig.9b we plot the electron density as a function of temperature around pseudo-critical temperature. We observe a tiny depression at T_p reminiscent of the pseudo-transition due to thermal excitations to states with a single electron per unit cell (see phase-diagram).

Similarly, the electron density is depicted in fig.9c as function of temperature in semi-logarithmic scale, assuming same set of parameters, but for $\mu = 1.28$. Once again electron density remains almost constant $\rho = 4/3$, for temperatures below $T \sim 0.01$, while for higher temperature there is a peak reaching $\rho \approx 4.20$. In fig.9d we present a zooming plot of panel (c) around the pseudo-critical temperature, where a tiny peak reminiscent of the pseudo-critical temperature is also present reflecting thermal excitations to states with 5 electrons per unit cell (see phase diagram). Surely we cannot expect any strong change in the electron density around T_p because the two competing ground state have equivalent electron densities.

V. SECOND-ORDER LIKE PSEUDO-TRANSITION

Now let us turn our attention to the second-order derivative of the free energy. The following quantities exhibit trends quite similar to second-order phase transition. It is important to reinforce that there is no singularity at T_p but just a rather sharp peak.

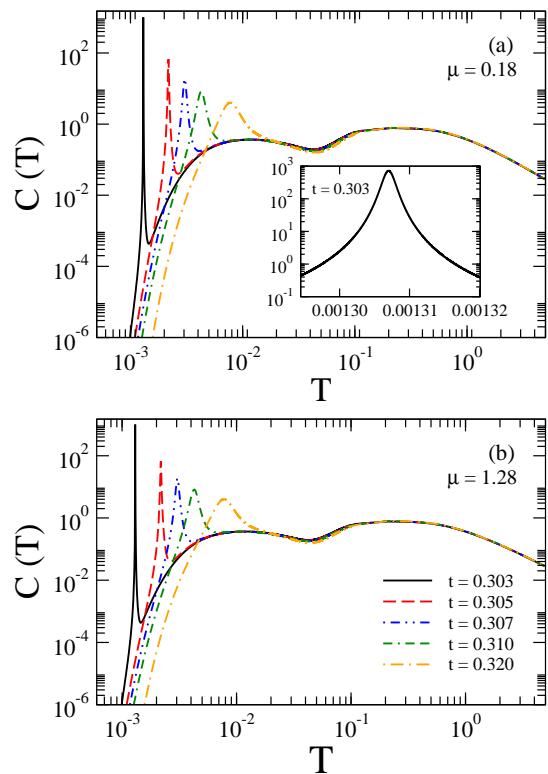


Figure 10: Specific heat as a function of temperature in logarithmic scale for $U = 1$ and $V = 0.1$. (a) For several values of t and $\mu = 0.18$ (in the vicinity of the $FRU_2 - AFM_2$ phase-boundary). Inset: zooming around T_p . (b) For several values of t and $\mu = 1.28$ (in the vicinity of the $FRU_4 - AFM_4$ phase-boundary).

A. The specific heat

In fig. 10, we display the specific heat $C = T \left(\frac{\partial \mathcal{S}}{\partial T} \right)$ as a function of temperature in logarithmic scale assuming fixed $U = 1$, $V = 0.1$. In panel (a) we depict for several values of t and $\mu = 0.18$ (close to the $FRU_2 - AFM_2$ ground-state transition). Here we see how the height of the peak increases and the peak becomes sharper when $t \rightarrow 0.3$, while for t larger the height of the peak becomes lower and broader. At low temperatures, we observe clearly a huge sharp peak quite similar to a second-order phase transition divergence around T_p . However, a zooming look as provided in the inner plot around T_p , evidences the rounded nature of the peak at the pseudo-critical temperature. Panel (b) reports the specific heat for the same set of parameters used in panel (a) but for $\mu = 1.28$ (close to the $FRU_4 - AFM_4$ ground-state phase transition).

Now let us analyze the nature of the peak around T_p , looking for some critical exponent universality. For this purpose, we consider the specific heat around pseudo-critical temperature in asymptotic limit (but not very close to T_p), which can be expressed according the discussion in reference [9] as

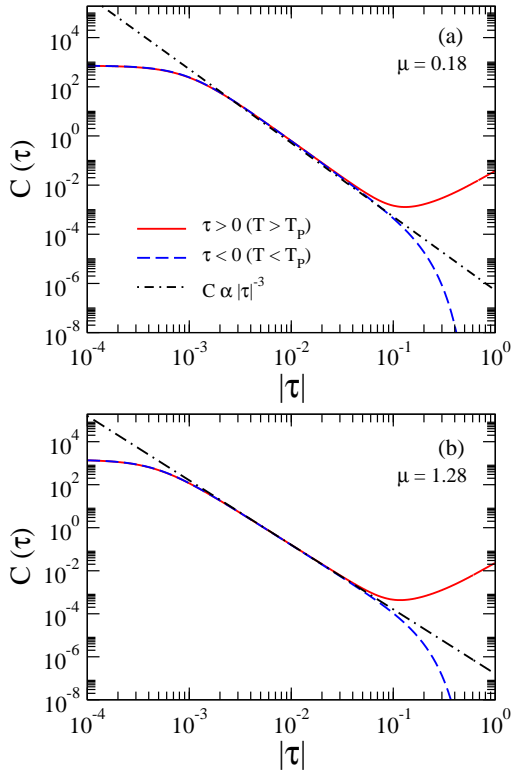


Figure 11: Logarithmic specific heat as a function of $\ln(|\tau|)$, for fixed parameters $U = 1$, $V = 0.1$, $t = 0.303$. Solid line corresponds for $\tau > 0$ ($T > T_p$) and dashed line denotes $\tau < 0$ ($T < T_p$). The straight dash-dotted line reports $\xi \propto |\tau|^{-3}$. (a) For $\mu = 0.18$. (b) For $\mu = 1.28$.

$$C(\tau) = T \left(\frac{\partial \mathcal{S}}{\partial \tau} \right) \left(\frac{\partial \tau}{\partial T} \right) \Big|_{T_p} = 2c_f \tau^{-3}, \quad (41)$$

where the coefficient c_f is given by

$$c_f = \begin{cases} \tilde{w}_{0,1}^2 c_{0,\xi}, & w_{0,0} \sim 2w_{1,1} \\ \tilde{w}_{1,2}^2 c_{2,\xi}, & w_{2,2} \sim 2w_{1,1} \end{cases}. \quad (42)$$

Therefore the specific heat has the following pre-asymptotic expression when approaching the pseudo-critical temperature

$$C(\tau) \propto |\tau|^{-\alpha}, \quad (43)$$

with critical exponent $\alpha = 3$. The Hubbard diamond chain in the atomic limit also satisfy the pseudo-critical exponent found in reference [9]. However, it is worth stressing that this pre-asymptotic regime is only valid around the ascending and descending parts of the peak, and surely fails very close to the peak top where the perturbation condition can not prevail.

In order to confirm the above result. We report in fig.11a the $C(\tau)$ as a function of τ , assuming fixed parameters $U = 1$, $V = 0.1$, $t = 0.303$ and $\mu = 0.18$ (near

the $AFM_2 - FRU_2$ phase-boundary). Continuous line represents data above T_p , while dashed line corresponds data below T_p . The dash-dotted line describes the asymptotic function, with critical exponent $\alpha = 3$. The straight line with angular coefficient $\alpha = 3$ fits accurately data over nearly two decades. Very close to T_p the power-law behavior breaks down, reflecting the actual analytic behavior of the specific heat. In panel (b) we plot the specific heat for $\mu = 1.28$ (near the $AFM_4 - FRU_2$ phase boundary), showing similar trends.

B. Compressibility

Another interesting quantity to be discuss is the isothermal electron compressibility[42] $\kappa_T = \frac{1}{\rho^2} \left(\frac{\partial \rho}{\partial \mu} \right)_T$, as a function of Hamiltonian parameters, temperature and electron density.

In fig.12a the isothermal compressibility is shown as a function of temperature in semi-logarithmic scale, we observe a tiny peak at the pseudo-critical temperature. Magnifying around the pseudo-critical temperature (see fig. 12b) it illustrated a double peak with local minimum at T_p . Since the pseudo-transition results from competing ground-states with the same electron density, we actually cannot expect any giant peak of the electron compressibility at T_p because that would result in a pronounced electron density change.

VI. SUMMARY AND CONCLUSIONS

In summary, we considered the extended Hubbard diamond chain restricted to the atomic limit with an arbitrary number of particles driven by chemical potential. The interaction between dimer diamond chain and nodal couplings are taken in the atomic limit (no hopping), while dimer interaction includes the hopping term. We showed that this model exhibits a pseudo-transition effect in the low-temperature region. The internal energy and entropy were shown to change quite abruptly in a very narrow range of temperatures around the pseudo-transition when the physical parameters are properly tuned in a close vicinity of special ground-state phase transitions. The correlation length and specific heat display pronounced peaks with well defined power-laws in a well defined temperature range in the vicinity of the pseudo-transition point. The pseudo-critical exponents associated with the correlation length and specific heat were shown to be $\nu = 1$ and $\alpha = 3$, respectively. These are the same pseudo-exponents reported to hold in spin models with Ising-like interactions, pointing towards a universal behavior of pseudo-transitions[9, 10]. We also demonstrated that the electron density and respective electronic compressibility displays reminiscent signatures of the pseudo-transition. The present results add to the general understanding of the remarkable phenomenon of

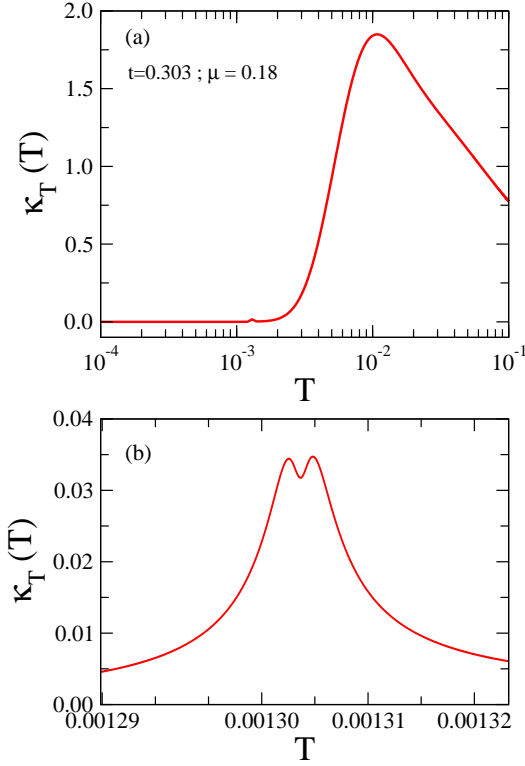


Figure 12: Isothermal compressibility as a function of temperature in semi-logarithmic scale, for fixed $t = 0.303$, $\mu = 0.18$, $U = 1$ and $V = 0.1$. (b) Magnified around T_p .

pseudo-transitions taking place at finite temperatures in one-dimensional equilibrium systems having structured interactions within the relevant unit cell.

VII. ACKNOWLEDGEMENTS

This work was supported by CAPES (Coordenação de Aperfeiçoamento de Pessoal de Nível Superior), CNPq (Conselho Nacional de Desenvolvimento Científico e Tecnológico), FAPEAL (Fundação de Apoio à Pesquisa do Estado de Alagoas), and FAPEMIG (Fundação de Apoio à Pesquisa do Estado de Minas Gerais).

Appendix A: Real roots of cubic equation

Transfer matrix is a symmetric matrix, so its eigenvalues are guaranteed to be real values. Therefore, here we verify the cubic equation (23) roots must be different and real numbers, given by (25).

Obviously, we can convince that both Q and R are real numbers from (27) and (28).

Now let verify the real number Q is positively defined by using the cubic equation coefficients (24), thus after some algebraic manipulation we obtain the following ex-

ϕ	Largest	2nd Largest	Lowest
$\langle 0, \pi \rangle$	Λ_0	Λ_1	Λ_2
$\langle \pi, 2\pi \rangle$	Λ_1	Λ_0	Λ_2
$\langle 2\pi, 3\pi \rangle$	Λ_1	Λ_2	Λ_0
$\langle 3\pi, 4\pi \rangle$	Λ_2	Λ_1	Λ_0
$\langle 4\pi, 5\pi \rangle$	Λ_2	Λ_0	Λ_1
$\langle 5\pi, 6\pi \rangle$	Λ_0	Λ_2	Λ_1

Table II: Cubic root solutions are tabulated in decreasing order by intervals in ϕ .

pression

$$Q = \frac{1}{9} (w_{2,2} - \frac{1}{2}w_{0,0} - w_{1,1})^2 + \frac{1}{12} (w_{0,0} - 2w_{1,1})^2 + \frac{2}{3}w_{0,1}^2 + \frac{1}{3}w_{0,2}^2 + \frac{2}{3}w_{1,2}^2, \quad (\text{A1})$$

which is strictly a positive number ($Q > 0$), since all Boltzmann factors are positive. According to a cubic equation property, this condition is enough to conclude that three the eigenvalues of transfer matrix will be different and real numbers.

Now the question is to determine which are the largest and the lowest eigenvalues? Since all eigenvalues must be real and different because $Q > 0$. Which implies that the solution (25), must satisfy the following restriction $\phi \neq \pm n\pi$, with $n = \{0, 1, 2, \dots\}$. Therefore, we can choose ϕ conveniently such that $0 < \phi < \pi$. Thus we have the following trigonometric relation

$$\cos\left(\frac{\phi}{3}\right) > \cos\left(\frac{\phi-2\pi}{3}\right) > \cos\left(\frac{\phi-4\pi}{3}\right), \quad (\text{A2})$$

if we multiply all terms of inequalities by $2\sqrt{Q} > 0$, and adding $-\frac{a_3}{3}$ to all expressions (note that $a_3 < 0$), thus we conclude that

$$\Lambda_0 > \Lambda_1 > \Lambda_2. \quad (\text{A3})$$

Note that if $\phi = 0$, in principle we would have $\Lambda_1 = \Lambda_2$ but this condition is forbidden because $Q > 0$. Similarly for $\phi = \pi$ we have $\Lambda_0 = \Lambda_1$, but again this condition cannot be satisfied since $Q > 0$. Therefore, we have identified which eigenvalues is the largest one and the lowest one.

Of course we can choose other intervals equivalently, and verify how the eigenvalues are ordered. In table II is reported the eigenvalues for each intervals. The open intervals of ϕ guaranties all eigenvalues must be real and different values, in order to satisfy the condition $Q > 0$.

The three cubic root solutions are exchanging periodically which depends on interval of ϕ , making a bit puzzle to identify which eigenvalues is the largest one. In table II it is reported how the eigenvalues are ordered. In each interval the solutions are equivalent, because other intervals simply exchange the eigenvalues with no relevance. Therefore, here we conveniently choose the first interval $\phi \in \langle 0, \pi \rangle$, so the eigenvalues must be ordered as follow $\Lambda_0 > \Lambda_1 > \Lambda_2$.

Even more, according to Perron-Frobenius theorem, the largest eigenvalue must be non-degenerate and positive.

Appendix B: Perturbative Transfer Matrix Correction

In order to study the pseudo-transitions property in low-temperature region, we need to analyze the transfer matrix in the low temperature region. In principle, cubic root solution could be a bit cumbersome task to identify as an easy handling solutions. A simple strategy to obtain a reasonable solution could be considering the transfer matrix (19), as a sum of two matrix $\mathbf{V} = \mathbf{V}_0 + \zeta \mathbf{V}_1$. The first term is given by

$$\mathbf{V}_0 = \begin{bmatrix} w_{0,0} & 0 & w_{0,2} \\ 0 & 2w_{1,1} & 0 \\ w_{0,2} & 0 & w_{2,2} \end{bmatrix}, \quad (\text{B1})$$

This matrix can be considered as the unperturbed transfer matrix, whose eigenvalues are

$$u_0^{(0)} = \frac{1}{2} [w_{0,0} + w_{2,2} + s], \quad (\text{B2})$$

$$u_1^{(0)} = 2w_{1,1}, \quad (\text{B3})$$

$$u_2^{(0)} = \frac{1}{2} [w_{0,0} + w_{2,2} - s], \quad (\text{B4})$$

where $s = \sqrt{d^2 + 4w_{0,2}^2}$ and $d = w_{0,0} - w_{2,2}$.

In the limit of $w_{0,2} \rightarrow 0$, the unperturbed solution can eventually satisfy the following relation

$$u_0^{(0)} = u_1^{(0)}. \quad (\text{B5})$$

This condition leads to a pseudo-transition, which we can simplify:

$$w_{0,0} = 2w_{1,1}, \quad \text{for } w_{0,0} > w_{2,2}, \quad (\text{B6})$$

$$w_{2,2} = 2w_{1,1}, \quad \text{for } w_{0,0} < w_{2,2}. \quad (\text{B7})$$

The above condition is essential to find pseudo-critical temperature T_p .

The second term of transfer matrix is given by

$$\mathbf{V}_1 = \begin{bmatrix} 0 & \sqrt{2}w_{0,1} & 0 \\ \sqrt{2}w_{0,1} & 0 & \sqrt{2}w_{1,2} \\ 0 & \sqrt{2}w_{1,2} & 0 \end{bmatrix}. \quad (\text{B8})$$

Close to the pseudo-critical temperature, the elements of matrix \mathbf{V}_1 become smaller than the elements of matrix \mathbf{V}_0 . Therefore, we can find the transfer matrix eigenvalues by using a perturbative approach.

Consequently, the solution of the transfer matrix after a standard perturbative manipulation up to first order term gives us the following root corrections,

$$u_0^{(1)} = \frac{[(s-d)w_{1,2} + 2w_{0,2}w_{0,1}]^2}{s(s-d)(u_0^{(0)} - 2w_{1,1})}, \quad (\text{B9})$$

$$u_1^{(1)} = -u_0^{(1)} - u_2^{(1)}, \quad (\text{B10})$$

$$u_2^{(1)} = \frac{[(s+d)w_{1,2} - 2w_{0,2}w_{0,1}]^2}{s(s+d)(u_2^{(0)} - 2w_{1,1})}. \quad (\text{B11})$$

As a consequence of the perturbative correction, the transfer matrix eigenvalues becomes

$$\Lambda_j = u_j^{(0)} + \zeta u_j^{(1)} + \mathcal{O}(\zeta^2), \quad j = \{0, 1, 2\}. \quad (\text{B12})$$

Assuming the elements of matrix V_1 are small, we can obtain an approximate result of (25), fixing $\zeta = 1$. Hence, it is evident that the largest eigenvalue of the transfer matrix will be Λ_0 , even when $u_0^{(0)} = u_1^{(0)}$, since $u_0^{(1)} > 0$ and $u_1^{(1)} < 0$.

-
- [1] S.M. de Souza and O. Rojas, Sol. State. Comm. **269**, 131 (2018).
[2] I.M. Carvalho, J. Torrico, S.M. de Souza, O. Rojas, and O. Derzhko, Ann. Phys. **402**, 45 (2019).
[3] J. Torrico, M. Rojas, S.M. de Souza, O. Rojas, and N.S. Ananikian, Eur. Phys. Lett. **108**, 50007 (2014).
[4] J. Torrico, M. Rojas, S.M. de Souza, and O. Rojas, Phys. Lett. A **380**, 3655 (2016).
[5] J. Strečka, Acta Phys. Pol. A **137**, 610 (2020).
[6] L. Galisova and J. Strečka, Phys. Rev. E **91**, 022134 (2015).
[7] O. Rojas, J. Strečka and S.M. de Souza, Sol. State. Comm. **246**, 68 (2016).
[8] J. Strečka, R.C. Alecio, M.L. Lyra, and O. Rojas, J. Magn. Magn. Mater. **409**, 124 (2016).
[9] O. Rojas, J. Strečka, M.L. Lyra, and S.M. de Souza, Phys. Rev. E **99**, 042117 (2019).
[10] T. Hutak, T. Krokhumalskii, O. Rojas, S.M. de Souza, and O. Derzhko, Phys. Lett. A **387**, 127020 (2021).
[11] I. Daruka and Z. Gulacsi, Phys. Rev. E **58**, 5403 (1998).
[12] I.S. Hagemann, Q. Huang, X.P.A. Gao, A.P. Ramirez, and R.J. Cava, Phys. Rev. Lett. **86**, 894 (2001).
[13] J. van Lierop and D.H. Ryan, Phys. Rev. Lett. **86**, 4390 (2001).
[14] O. Derzhko, A. Honecker and J. Richter, Phys. Rev. B **79**, 054403 (2009).
[15] O. Derzhko, J. Richter, A. Honecker, M. Maksymenko, and R. Moessner, Phys. Rev. B **81**, 014421 (2010).

- [16] O. Derzhko and J. Richter, Phys. Rev. B **90**, 045152 (2014).
- [17] R.R. Montenegro-Filho and M.D. Coutinho-Filho, Phys. Rev. B **74**, 125117 (2006).
- [18] R.R. Montenegro-Filho, F.S. Matias and M.D. Coutinho-Filho, Phys. Rev. B **102**, 035137 (2020).
- [19] Z. Gulácsi, A. Kampf and D. Vollhardt, Phys. Rev. Lett. **99**, 026404 (2007); Prog. Theor. Phys. Suppl. **176**, 1 (2008).
- [20] O. Rojas, S.M. de Souza and N.S. Ananikian, Phys. Rev. E **85**, 061123 (2012).
- [21] O. Krupnitska, Phys. Rev. B **102**, 064403 (2020).
- [22] J. Torrico, M. Rojas, M.S.S. Pereira, J. Strečka, and M.L. Lyra, Phys. Rev. B **93**, 014428 (2016).
- [23] B. Nachtergaele, J.P. Solovej and J. Yngvason, *Condensed Matter Physics and Exactly Soluble Models*, Selected of E.H. Lieb, (Springer, Berlin-Heidelberg, 2004).
- [24] G. Beni and P. Pincus, Phys. Rev. B **9**, 2963 (1974).
- [25] F. Mancini, Eur. Phys. J. B **47**, 527 (2005).
- [26] F. Mancini and F.P. Mancini Phys. Rev. E **77**, 061120 (2008).
- [27] O. Rojas and S.M. de Souza, Phys. Lett. A **375**, 1295 (2011).
- [28] A.A. Lopes and R.G. Dias, Phys. Rev. B **84**, 085124 (2011).
- [29] B.M. Lisnii, Low Temp. Phys. **37**, 296 (2011).
- [30] K.C. Rule, A.U.B. Wolter, S. Sullow, D.A. Tennant, A. Bruhl, S. Kohler, B. Wolf, M. Lang, and J. Schreuer, Phys. Rev. Lett. **100**, 117202 (2008).
- [31] H. Kikuchi, Y. Fujii, M. Chiba, S. Mitsudo, T. Idehara, T. Tonegawa, K. Okamoto, T. Sakai, T. Kuwai, and H. Ohta, Phys. Rev. Lett. **94**, 227201 (2005); H. Kikuchi, Y. Fujii, M. Chiba, S. Mitsudo, T. Idehara, T. Tonegawa, K. Okamoto, T. Sakai, T. Kuwai, A. Matsuo, W. Higemoto, K. Nishiyama, M. Horvati?, and C. Bertheir, Prog. Theor. Phys. Suppl. **159**, 1 (2005).
- [32] L. Canova, J. Strecka and M. Jascur, J. Phys.: Condens. Matter **18**, 4967 (2006).
- [33] N.S. Ananikian, L.N. Ananikian, L.A. Chakhmakhchyan, and O. Rojas, J. Phys.: Condens. Matter **24**, 256001 (2012).
- [34] L. Chakhmakhchyan, N. Ananikian, L. Ananikian, and C. Burdik, J. Phys: Conf. Series **343**, 012022 (2012).
- [35] Sh.-S. Deng, Sh.-J. Gu, and H.-Q. Lin, Phys. Rev. B **74**, 045103 (2006).
- [36] M.S.S. Pereira, F.A.B.F. de Moura and M.L. Lyra, Phys. Rev. B **77**, 024402 (2008); Phys. Rev. B **79**, 054427 (2009).
- [37] H. Jeschke, I. Opahle, H. Kandpal, R. Valenti, H. Das, T. Saha-Dasgupta, O. Janson, H. Rosner, A. Bruhl, B. Wolf, M. Lang, J. Richter, S. Hu, X. Wang, R. Peters, T. Pruschke, and A. Honecker, Phys. Rev. Lett. **106**, 217201 (2011).
- [38] B. Gu and G. Su, Phys. Rev. B **75**, 174437 (2007); O. Derzhko and J. Richter, Eur. Phys. J. B **52**, 23 (2006).
- [39] M. Cui, N. Wang, S. Zhang, and Z. He, Crystal Growth & Design **19**, 547 (2019).
- [40] A. Honecker and A. Lauchli, Phys. Rev. B **63**, 174407 (2001).
- [41] O. Rojas, Chi. Jour. Phys. **70**, 157 (2021).
- [42] R.J. Baxter, *Exactly Solved Models in Statistical Mechanics*, (Academic Press, New York, 1982).
- [43] Y. Saito, Prog. Theor. Phys. **59**, 375 (1978).